Carbonate associated uranium isotopes as a novel local redox indicator in oxidatively disturbed reducing sediments

Matthew O. Clarkson [a,*], Rick Hennekam [a,b], Tim C. Sweere [a], Morten B. Andersen [c], Gert-Jan Reichart [b,d], Derek Vance [a]

[a] *Department of Earth Sciences, ETHZ, Zurich 8092, Switzerland*
[b] *Department of Ocean Systems, NIOZ Royal Netherlands Institute for Sea Research, 't Horntje 1797 SZ, the Netherlands*
[c] *School of Earth and Environmental Sciences, University of Cardiff, Cardiff CF10 3AT, UK*
[d] *Department of Earth Sciences, Utrecht University, 3584 CB Utrecht, the Netherlands*

Abstract

The interpretation of local redox indicators in marine sediments relies on their preservation. By their nature, such biogeochemical tracers are susceptible to diagenetic alteration, particularly through post-depositional re-oxidation of the sediment. This can result in the mobilization and loss of distinctive redox dependant signatures, leading to the classical problem that the presence of oxygenated conditions cannot be robustly inferred by the absence of evidence for anoxia. Authigenic uranium enrichments, and their isotope signatures ($\delta^{238}U$), are widely used to infer bottom-water and pore-water redox conditions but are susceptible to later oxidative diagenetic disturbance. Here we explore the preservation of authigenic $\delta^{238}U$ signatures in sediment samples from Sapropel S1 at Site 64PE406-E1 in the Eastern Mediterranean Sea (~1760 m water depth), which was originally deposited under reducing conditions but severely affected by later oxidative diagenesis and the variable loss of authigenic U(IV) from the upper sapropel. To this end, we compare U isotope signatures from bulk measurements ($\delta^{238}U_{bulk}$) with detrital corrected authigenic U ($\delta^{238}U_{auth}$) and carbonate associated U ($\delta^{238}U_{CAU}$). In contrast to open ocean carbonates deposited under fully oxic conditions, sapropelic carbonate leachates yield $\delta^{238}U_{CAU}$ similar to calculated $\delta^{238}U_{auth}$, thus recording (predominantly) redox dependant isotope fractionation. There is no evidence for significant isotope fractionation resulting from post-depositional oxidative diagenesis, but associated authigenic U(IV) removal results in larger relative detrital contributions to $\delta^{238}U_{bulk}$, and hence large uncertainties on $\delta^{238}U_{auth}$ estimates. By contrast, $\delta^{238}U_{CAU}$ successfully avoids detrital phases, and the uncertainty associated with detrital corrections, providing a primary record of changes in local redox conditions. Thus, we propose that $\delta^{238}U_{CAU}$ can be used for accurate reconstructions of benthic de-oxygenation in sediments with low U enrichments, including sediments with post-depositional U(IV) loss and less reducing environments.
© 2021 The Author(s). Published by Elsevier Ltd. This is an open access article under the CC BY-NC-ND license (http://creativecommons.org/licenses/by-nc-nd/4.0/).

Keywords: Uranium isotopes; Sapropel; Oxidative diagenesis; Burn-down

1. INTRODUCTION

The presence of reducing conditions in marine settings has major implications for biotic evolution, mass extinctions and global biogeochemical cycles, making it the subject of significant research effort. Several tools are available to identify the presence and severity of local

* Corresponding author.
E-mail address: matthew.clarkson@erdw.ethz.ch (M.O. Clarkson).

de-oxygenation within the water column or at the sediment–water interface and these have been applied across the entirety of the geological record (see Meyer and Kump, 2008; Lyons et al., 2009; Kendall, 2020). These methods are highly diverse and include sedimentological parameters (e.g., laminations, pyrite framboid counts), palaeontological patterns (e.g. faunal turnover and ichnofabrics), organic (e.g. organic carbon enrichments, biomarkers) and inorganic geochemistry (e.g. trace metal speciation, enrichment factors or isotope signatures) (Canfield et al., 1992; Koopmans et al., 1996; Slomp et al., 1996; Twitchett and Wignall, 1996; Wignall and Newton, 1998; Poulton et al., 2004; Tribovillard et al., 2006; Andersen et al., 2017; Raiswell et al., 2018; Algeo and Liu, 2020). Each approach has strengths and weaknesses, but together they capture different temporal, spatial or biogeochemical aspects of the redox environment. A major challenge for using these tools, however, lies in their preservation. By their nature, redox-driven biogeochemical signatures are delicate and can be removed, modified or obscured by early diagenesis, particularly through the post-depositional oxidation of the anoxically-deposited sediment (i.e., 'burn-down'; Jung et al., 1997; Thomson et al., 1998; Reed et al., 2011). Consequently, whilst evidence can be found to robustly indicate oxygen depletion, the absence of such evidence is not conclusive.

The loss of distinctive biogeochemical signatures to oxidative diagenesis is especially problematic in settings with temporally variable intensities of reducing conditions, low organic carbon enrichments, low sedimentation rates or high porosity (Jung et al., 1997; Reed et al., 2011). A classic example of the impacts of oxidative diagenesis is the Mediterranean Sapropel S1; an organic carbon-rich layer deposited between ~10.5 and 6.1 cal. kyr BP as a consequence of increased productivity and/or water-column stagnation in the eastern Mediterranean Sea (Rohling et al., 2015; Grant et al., 2016). The oxidative loss of organic carbon (Higgs et al., 1994; Van Santvoort et al., 1996) and redistribution or complete removal of redox sensitive trace metals from the sediment (Thomson et al., 1995) obscure the identification of upper sapropel conditions. In some instances, the sapropel can be completely lost from the sedimentary record, resulting in 'ghost sapropels' (Rohling et al., 2015). In circumstances where the characteristic elevations in organic carbon have been lost, enhanced barite accumulation can still be used to infer a high productivity event and define the sapropel interval (Thomson et al., 1995; Van Santvoort et al., 1996; Thomson et al., 1999; De Lange et al., 2008), but this does not constrain the degree of contemporary redox changes. As a result, it is difficult to de-convolve the competing controls on oxygen depletion (via aerobic respiration of organic matter), oxygen solubility (controlled by temperature) and oxygen supply (via ventilation).

Authigenic U enrichments, above background detrital concentrations, are widely used to identify the presence of reducing conditions at or below the sediment–water interface, reflecting the reduction of soluble U(VI) to insoluble U(IV) (McManus et al., 2006; Tribovillard et al., 2006; Jacobel et al., 2020). Uranium reduction is generally associated with the preferential enrichment of ^{238}U over ^{235}U, leading to high sedimentary $\delta^{238}U$ values that are diagnostic of reducing environments (Stirling et al., 2007; Weyer et al., 2008; Montoya-Pino et al., 2010; Tissot and Dauphas, 2015; Rolison et al., 2017), although the precise expression of the magnitude of isotope enrichment is often more complex (Andersen et al., 2014; Brüske et al., 2020; Lau et al., 2020). Authigenic U(IV) is, however, highly susceptible to oxidative remobilization and redistribution (Zheng et al., 2002; Morford et al., 2009) and the impact of this on sedimentary $\delta^{238}U$ values remains untested. In particular, complications associated with oxidatively disturbed sediments may relate to i) the potential for U isotope fractionation during oxidation and/or reprecipitation with metal oxides or residual solids (Brennecka et al., 2011; Wang et al., 2015) and ii) the diminished size of the authigenic U pool relative to lithogenic components, leading to increased uncertainties in detrital-corrected authigenic $\delta^{238}U$ ($\delta^{238}U_{auth}$) estimates (Andersen et al., 2016; Andersen et al., 2020).

Carbonate associated U isotopes ($\delta^{238}U_{CAU}$) may offer an alternative tool for local redox reconstructions. The co-precipitation of U(VI) in carbonates under oxic conditions generally results in limited U isotope fractionation (Chen et al., 2016; Chen et al., 2018b) and $\delta^{238}U_{CAU}$ are often used to reconstruct past seawater compositions, tracking global-scale changes in seafloor anoxia (see Zhang et al., 2020 for review). Under anoxic conditions, however, U(IV) is readily incorporated into the carbonate lattice (Sturchio et al., 1998; Zhao et al., 2016). Indeed, U(IV) enrichments in carbonate phases are thought to semi-quantitatively track overall authigenic U enrichments in pelagic sediments (Boiteau et al., 2012; Gottschalk et al., 2016) and record the associated heavy isotope compositions associated with U reduction (Romaniello et al., 2013; Chen et al., 2018a; Tissot et al., 2018; Chen et al., 2021; Clarkson et al., 2021). With the isotope signature preserved in the carbonate lattice, it might better escape the impacts of post-depositional oxidative mobilization. Moreover, the selective isolation of the carbonate phase from a bulk sediment (e.g., Clarkson et al., 2020) avoids the uncertainties associated with detrital corrections for $\delta^{238}U_{auth}$ estimates.

Here we examine the utility of $\delta^{238}U$, in general, as a redox indicator in oxidatively disturbed sediments using bulk measurements ($\delta^{238}U_{bulk}$), $\delta^{238}U_{auth}$ and $\delta^{238}U_{CAU}$. For this purpose, we focus on the well-understood Sapropel S1, using samples from core 64PE406-E1 in the eastern Mediterranean Sea (~1760 m water depth), which shows clear evidence of partial re-oxidation in the upper part of S1 (see Section 3). Comparison is then made to published $\delta^{238}U_{auth}$ from a nearby, deeper locality at ODP Site 967 (Andersen et al., 2020). The Site 967 core shows less post-depositional re-oxidation so that $\delta^{238}U_{auth}$ values are expected to be less impacted by oxidative U(IV) mobilization for the upper part of the sapropel compared to our site. The aims of this study are to i) assess if $\delta^{238}U_{CAU}$ is representative of $\delta^{238}U_{auth}$ and can accurately capture the same (predominantly) redox-dependant U isotope fractionation, and ii) examine the preservation of these signatures in a setting where oxidative diagenesis has clearly removed U(IV)

from the sediment. We use a framework of very high-resolution bulk U/Al, Mn/Al, and Ba/Al data to precisely identify the periods of enhanced local productivity, the oxidized intervals and the better-preserved sapropel intervals.

2. METHODS

2.1. Site description, sediment material, and chronology

A piston core (PC) and multicore (MC) were recovered at site 64PE406-E1 (33°18.1′N, 33°23.7′E) at 1760 m water depth (Bale et al., 2019; Hennekam et al., 2020; Sweere et al., 2021) during cruise 64PE406 on R/V Pelagia in 2016. Core material is composed of calcite rich hemipelagic oozes, with distinct dark bands indicating sapropel layers (Bale et al., 2019). This core location lies just above the 1800 m depth mark, inferred to be the depth rarely reached by convective turnover during Sapropel S1 (De Lange et al., 2008), and likely subjected to variable redox conditions during deposition compared to deeper localities. The MC at site 64PE406-E1 contains a near complete Sapropel S1 interval, overlain by a continuous record to present, while the PC contains the lowermost ~2 cm of sapropel S1 only, underlain by Early Holocene to Pleistocene sediments. For simplicity we assume the cores to be contiguous, providing a near-continuous Sapropel S1 record, which has been dated (Hennekam et al., 2020; Sweere et al., 2021) by careful alignment of sapropel boundaries and associated Ba/Al variability to a nearby core (LC21; Grant et al., 2016). Moreover, we use the commonly observed minimum in Ba/Al as an additional age control point, dated to be around ~8.5–7.8 kyr (Hennekam et al., 2014; Rohling et al., 2015). In order to facilitate the best comparison to the nearby Site 967 data (Andersen et al., 2020), we have re-aligned the data from this core location using the same chronological constraints as for our 64PE406-E1 site. Based on these age models, sedimentation rates vary between ~3 and 4 cm kyr^{-1} throughout the 64PE406-E1 record, and are generally higher for ODP Site 967, up to ~16 cm kyr^{-1}.

2.2. Bulk sediment calibrated XRF-CS

The 64PE406-E1 core was scanned for its bulk geochemistry, at a mm resolution, using X-Ray Fluorescence core scanning (XRF-CS) with an Avaatech XRF Core Scanner at the NIOZ (see Hennekam et al., 2020). These high-resolution geochemical data were converted to concentrations using a multivariate log-ratio approach (Weltje et al., 2015), which effectively converts the XRF-CS intensity data to concentration data obtained by inductively coupled plasma mass spectrometry (ICP-MS). For calibration, discrete sediment samples from site 64PE406-E1 were dried, powdered, and digested (~100–125 mg) in an HClO$_4$-HNO$_3$-HF acid mixture (following Reitz et al., 2006). The digested samples were converted to 1 M HNO$_3$ and measured with a Thermo Scientific Element 2 ICP-MS at the NIOZ, with an internal indium (In) standard and a blank correction applied. Standard samples (MESS-3 and JSd-3) showed the following accuracy/precision (deviation from

reference value; 1RSD) for the ICP-MS measurements: Al (<5%/±1%), Mn (<2%/±3%), Ba (<6%/±1%), U (<4%/±2%).

2.3. Uranium concentration and isotope analysis

XRF-CS calibration sample digests make up part of the sample set used for further element and isotope analyses. Additional bulk sediment digests were performed at ETHZ on 50 mg sample powders using concentrated HNO$_3$ + HF, followed by treatment with aqua regia, each at 140 °C for 24 hrs, before dissolution in 1 M HCl. To selectively isolate the bulk carbonate fraction, approximately 300 mg of dry sample powder was leached using 40 mL of 1 M ammonium acetate (pH 5) for 24 hrs at room temperature (Clarkson et al., 2020). Leachates and digest solutions were directly aliquoted and diluted 400 times in 2% HNO$_3$. Major and trace elements were measured using a Thermo–Finnigan Element XR ICP–MS at ETHZ, using an internal In standard. Concentrations were calculated relative to an in-house, well characterized and gravimetrically produced, artificial standard with matrix characteristics similar to the samples. For carbonate leachates, U concentrations are reported normalized to Ca (μmol/mol) and as ppb for bulk sediment digests. Uncertainties on Ca and U concentrations are twice the relative standard deviation (RSD) of an in-house matrix matched secondary standard, which are typically ~10 and 7% respectively.

Uranium was isolated from matrix elements for both bulk digests and carbonate leachates using the RE-resin (Triskem) ion exchange chromatography methods described in Clarkson et al. (2020). Isotope ratios were measured at ETHZ on a Neptune Plus (Thermo– Finnigan) MC–ICPMS equipped with an Aridus II DSN (CETAC) and a PFA nebulizer and spray chamber (CPI) sample introduction system. Given the low U concentrations in the leachates 'jet + X-cones' were used to maximise the U transmission efficiency. Uranium isotope ratios are reported relative to the standard CRM-145 = 0‰ for ^{238}U/^{235}U and secular equilibrium for ^{234}U/^{238}U, and presented as:

$$\delta^{238}U = \left[\left({}^{238}U / {}^{235}U_{sample} \right) / \left({}^{238}U / {}^{235}U_{CRM145} \right) - 1 \right] * 1000 \tag{1}$$

$$\delta^{234}U = \left[\left({}^{234}U / {}^{238}U_{sample} \right) / \left({}^{234}U / {}^{238}U_{sec.\ eq} \right) - 1 \right] * 1000 \tag{2}$$

Internal errors (2SE) for δ^{238}U measurements were typically ± 0.02–0.04‰ at ion beam intensities of ~35 to 40 V (using 10^{11} ohm resistors) for ~40 ppb solutions. We used three secondary standards to assess external reproducibility and accuracy. Uncertainties are reported as the 2SD of a uraninite standard CZ-1 (purified in the same manner as samples and run every 5 samples) from the same session as the samples (±0.05–0.08‰) which is slightly larger than the long-term reproducibility of CZ-1 at ETHZ with this instrument setup (±0.06‰). We also ran replicates of the NIST SRM-1d argillaceous limestone (leached with

1 M HCl) which gives $\delta^{238}U$ of $-0.13 \pm 0.05\permil$ (2SD, n = 11) over the entire measurement period, similar to previously reported values (Dahl et al., 2017; Clarkson et al., 2020; del Rey et al., 2020), and the USGS shale standard SDO-1, which gave $-0.08 \pm 0.05\permil$ (n = 8), within error of published measurements (Kendall et al., 2015).

3. RESULTS

3.1. Calcium concentrations

Calcium makes up between 11.4 and 18.6 wt% of the bulk samples (Table 1), equivalent to ~28–46 % $CaCO_3$. There is a minor Ca decrease in sapropelic samples that likely reflects the dilution of carbonate by organic matter. Absolute Ca concentrations for the 1 M ammonium acetate leachates are within error (2RSD = 10%) of the bulk measurements (Table 2) and show similar stratigraphic trends, demonstrating near complete dissolution of the carbonate fraction.

3.2. Calibrated XRF-CS

High resolution calibrated XRF-CS data (Table S1; Fig. 1) demonstrate several typical geochemical features of Sapropel S1 that are seen elsewhere in the eastern Mediterranean basin (Mercone et al., 2000; Mercone et al., 2001; De Lange et al., 2008). Sapropel S1 can clearly be identified from the presence of the double Ba/Al peak, which indicates enhanced barite formation as a result of heightened productivity, and its flux to the seafloor (Bishop, 1988). The two Ba/Al peaks are separated by a minimum that marks the well-known interruption of Sapropel S1 at ~8.5–7.8 cal. kyr BP (Rohling et al., 2015), where productivity was lower and convective turnover temporarily ventilated the water column to at least ~1500–1800 m depth (Abu-Zied et al., 2008; De Lange et al., 2008). Importantly, barite is thought to be mostly immobile during later diagenesis, including the oxidation of organic matter (Thomson et al., 1995), so that it can be used to identify the S1 interval where organic carbon has been re-oxidized. By contrast, U/Al only shows significant enrichments (up to 3.3 ppm/wt% from a pre-sapropel background of ~0.3 ppm/wt%) during the lower part of S1 (30–36 cm), and returns to background values in the upper sapropel, indicative of oxidative U loss. In the upper sapropel, there is a coeval increase in Mn/Al (up to ~2200 ppm/wt% compared to the sapropel background of ~90 ppm/wt%), related to the reductive dissolution and re-precipitation of Mn-oxides. The Mn/Al record resolves at least two distinct peaks, where the lower peak is thought to mark the active oxidation front (Thomson et al., 1999). Elsewhere, a total organic carbon decrease occurs coeval with the Mn peak (De Lange et al., 2008), indicating the oxidative loss of organic carbon from the sediment. The simultaneous increase in U/Al with Ba/Al at the onset of S1 (De Rijk et al., 1999), suggests that this initial U enrichment is related to original depositional conditions, rather than a 'secondary' U peak driven by remobilization below the oxidation front. The decrease in U/Al begins before the interruption event and continues across the second Ba/Al peak, suggesting that U has been lost via oxidation but with no clear secondary redistribution peak deeper in the sediment.

3.3. Uranium isotopes

In post-S1 samples, $\delta^{238}U_{CAU}$ is invariant at $-0.38 \pm 0.06\permil$ (Table 2, Fig. 1), which is similar to modern seawater ($-0.39 \pm 0.01\permil$; Andersen et al., 2017). Before and during S1, $\delta^{238}U_{CAU}$ shows higher values that are typical of U reduction. Before S1, $\delta^{238}U_{CAU}$ is higher than seawater ($-0.21\permil$) and increases at the onset of S1, to a maximum $+0.69 \pm 0.06\permil$. For the remainder of the S1 record $\delta^{238}U_{CAU}$ is relatively high (-0.05 to $+0.38\permil$) and shows a striking correspondence to trends in Ba/Al from high resolution XRF-CS, both within the well-preserved and re-oxidized S1 intervals (Fig. 1). The $\delta^{238}U_{CAU}$ record also shows a minor decrease during the S1 interruption, as identified by Ba/Al (Fig. 1). In contrast to $\delta^{238}U_{CAU}$, $\delta^{238}U_{bulk}$ generally follows patterns in U/Al rather than Ba/Al (Fig. 1), with values up to $+0.47 \pm 0.07\permil$ at the start of S1 and a gradual decrease ($+0.23$ to $-0.33\permil$) through the remainder of the record. Pre- and post-sapropel samples record $\delta^{238}U_{bulk}$ (-0.40 to $-0.34\permil$) that are between Upper Continental Crust (UCC) values ($-0.29 \pm 0.03\permil$; Tissot and Dauphas, 2015) and modern seawater, likely reflecting the mixture of carbonate and detrital components (Figs. 1 and 2). All carbonate leachates show $\delta^{234}U$ values ($145 \pm 7\permil$; 1SD) close to modern seawater whereas the bulk digests show a large range of $\delta^{234}U$, between -9 and $118\permil$ (Tables 1 and 2, Fig. 2).

4. DISCUSSION

4.1. $\delta^{238}U$ and $\delta^{234}U$ relationships

In younger marine sediments (with little post-sedimentation decay of ^{234}U, whose half-life is ~246 ky) $\delta^{234}U$ can be used to distinguish between authigenic and detrital U phases (Holmden et al., 2015; Andersen et al., 2016; Bura-Nakić et al., 2018) and provide a useful framework to examine the variations in $\delta^{238}U$ for both bulk and carbonate measurements. In the following we discuss $\delta^{234}U$ and $\delta^{238}U$ as a function of U concentrations and ratios to Ca, using reciprocal concentrations and ratios (1/U and Ca/U) in Fig. 2 in order to better identify mixing (producing linear correlations) of detrital and authigenic components. Bulk measurements show a large range of $\delta^{234}U$ (Fig. 2a; -9 to $118\permil$) and an approximately linear correlation with 1/U. Samples with the lowest U concentrations have $\delta^{234}U$ close to or below secular equilibrium ($0\permil$), indicating that they are dominated by lithogenic components. Values of $\delta^{234}U$ below secular equilibrium are typical of pelagic sediments, and likely a result of the early diagenetic alpha-recoil loss of ^{234}U (DePaolo et al., 2006). By contrast, samples with higher U concentrations have more seawater-like $\delta^{234}U$ (~146‰; Andersen et al., 2010), signifying larger authigenic enrichments. In comparison to bulk

Table 1
U isotope, major and trace element data for bulk digests.

Zone	Total Depth (cm)	Age (kyrs)	$\delta^{238}U_{bulk}$ (‰)	2SD	$\delta^{234}U_{bulk}$ (‰)	2SE	U (ppm)	Al (wt%)	Ca (wt%)	Th/U (ppm/ppm)
Post S1	1.50	0.458	−0.40	0.07	6	1	1.42	4.01	14.36	3.76
Post S1	5.50	1.678	−0.38	0.07	15	1	1.19	3.54	18.56	4.29
Post S1	9.50	2.898	−0.35	0.07	19	1	1.21	3.76	17.14	4.46
Post S1	13.50	4.118	−0.38	0.07	14	1	1.32	3.05	14.92	3.74
Post S1	16.50	5.033	−0.36	0.07	15	1	1.30	3.03	12.93	3.75
S1 termination	19.50	5.948	−0.33	0.07	15	1	1.42	4.33	13.72	4.40
S1 termination	20.50	6.231	−0.29	0.07	21	1	1.44	3.62	13.25	4.06
S1 oxidized	22.50	6.756	−0.20	0.06	26	1	1.60	5.47	13.94	ND
S1 oxidized	23.50	7.019	ND	ND	ND	ND	ND	ND	ND	ND
S1 oxidized	24.50	7.281	−0.14	0.06	44	1	1.65	5.35	14.33	ND
S1 oxidized	26.50	7.806	−0.09	0.07	53	1	1.99	4.34	13.06	3.13
S1 oxidized	28.50	8.331	−0.11	0.06	55	1	1.84	5.36	13.59	ND
S1 residual	29.50	8.594	0.01	0.06	79	1	3.08	5.31	12.08	ND
S1 residual	30.50	8.856	0.06	0.06	87	1	3.11	2.84	11.88	ND
S1 residual	31.50	9.119	0.14	0.06	91	1	3.89	5.74	12.45	ND
S1 residual	32.50	9.381	0.25	0.06	114	1	8.16	4.23	13.37	0.74
S1 onset	33.75	9.775	0.46	0.07	118	1	8.06	5.52	11.82	ND
S1 onset	36.00	10.207	0.33	0.07	117	1	8.56	3.40	14.09	0.73
Pre S1	38.00	10.978	−0.36	0.07	18	1	1.85	2.78	11.39	2.42
Pre S1	40.00	11.775	−0.34	0.07	−9	1	1.36	3.43	16.44	ND

ND = not determined.

Table 2
U isotope, major and trace element data for carbonate leachates.

| Zone	Total Depth (cm)	Age (kyrs)	$\delta^{238}U_{CAU}$ (‰)	2SD	$\delta^{234}U_{CAU}$ (‰)	2SE	U/Ca (μmol/mol)	Ca (wt%)
Post S1	1.50	0.458	−0.36	0.08	137	1	0.36	13.07
Post S1	5.50	1.678	−0.39	0.08	141	1	0.29	15.75
Post S1	9.50	2.898	−0.38	0.05	150	1	0.24	17.26
Post S1	13.50	4.118	−0.39	0.08	139	1	0.28	15.42
Post S1	16.50	5.033	−0.30	0.08	137	1	0.33	12.65
S1 termination	19.50	5.948	−0.05	0.05	147	1	0.34	13.78
S1 termination	20.50	6.231	−0.05	0.08	137	1	0.41	11.89
S1 oxidized	22.50	6.756	0.19	0.08	148	1	0.56	11.70
S1 oxidized	23.50	7.019	0.20	0.05	154	1	0.50	12.31
S1 oxidized	24.50	7.281	0.31	0.05	157	1	0.56*	12.23*
S1 oxidized	26.50	7.806	0.25	0.05	166	1	0.65	12.15
S1 oxidized	28.50	8.331	0.16	0.05	145	1	0.64	11.66
S1 residual	29.50	8.594	0.32	0.05	145	1	1.37	10.39
S1 residual	30.50	8.856	0.27	0.05	145	1	2.19	10.35
S1 residual	31.50	9.119	0.38	0.05	144	1	2.41	10.31
S1 residual	32.50	9.381	0.36	0.05	137	1	6.10	10.70
S1 onset	33.75	9.775	0.69	0.05	140	1	9.40	11.08
S1 onset	36.00	10.207	0.52	0.05	143	1	4.97	12.28
Pre S1	38.00	10.978	−0.22	0.05	148	1	0.74	11.80
Pre S1	40.00	11.775	−0.20	0.05	144	1	0.50*	13.59*

* Interpolated from surrounding samples.
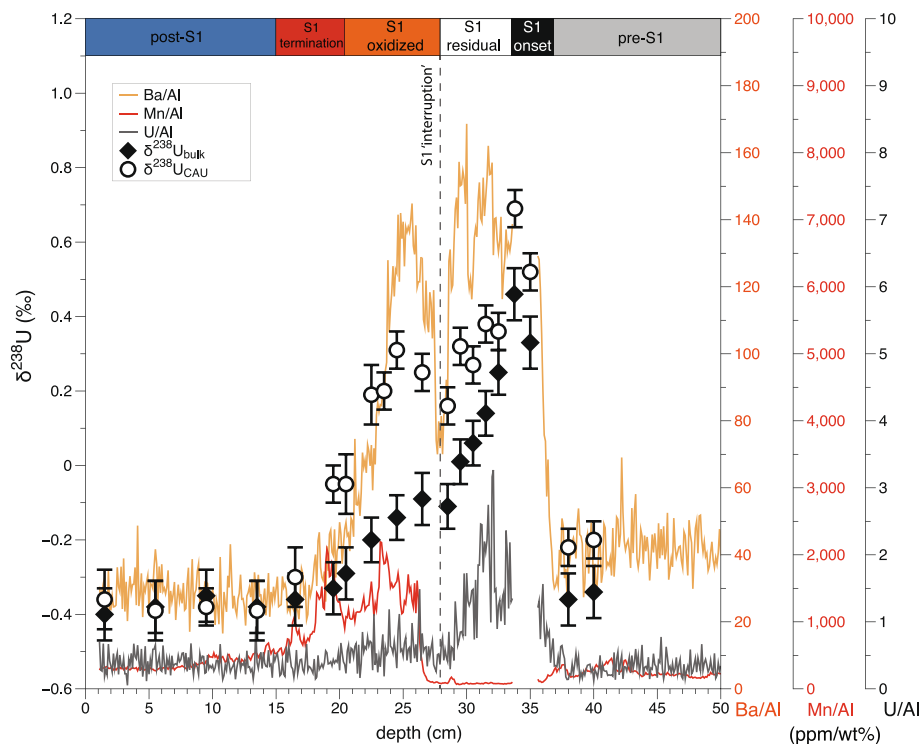
Fig. 1. Summary of bulk XRF-CS data and U isotope data for Sapopel S1, Site 64PE406-E1. High resolution XRF-CS data (ppm/wt%) show the distinct Ba/Al (orange line) double peak that is typical of S1. U/Al (black line) indicates U enrichment during the lower part of S1, but a loss of U in the upper part, which is coincident with a distinct Mn/Al peak. Carbonate (circles) and bulk (diamonds) $\delta^{238}U$ data show clear differences throughout the record and especially during the re-oxidized interval, reflecting significant detrital contributions to the bulk measurements. Oxidation of the core likely occurred during the sapropel interruption, and more extensively during and after S1 termination. Coloured bar (top) refers to zones of S1 that are used in later figures. (For interpretation of the references to colour in this figure legend, the reader is referred to the web version of this article.)
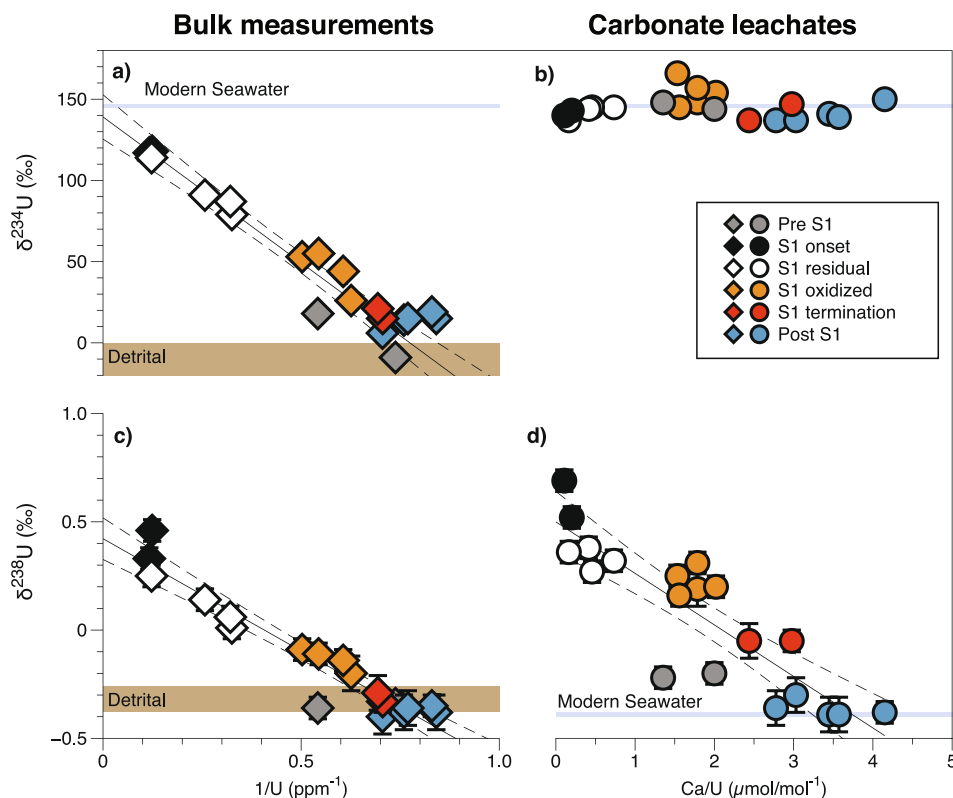
Fig. 2. Cross plots examining the relationship of $\delta^{234}U$ and $\delta^{238}U$ with U concentrations. (a) $\delta^{234}U$ plotted as a function of reciprocal U concentrations for bulk measurements. The near-linear correlation in (a) indicates that the samples contain a mixture of detrital and authigenic U. (b) $\delta^{234}U$ for carbonate leachates that are all close to modern seawater (blue shading). (c) $\delta^{238}U$ for bulk measurements as a function of reciprocal U concentrations, demonstrating the incorporation of authigenic U(IV) into sapropelic samples. (d) $\delta^{238}U$ for carbonate leachates showing a similar relationship to (c). Linear regressions shown with 95% confidence interval in (a), (c) and (d) and excluding post-S1 samples in a), where the higher contribution of carbonate phases leads to slightly higher $\delta^{234}U$ than detrital phases and lower U concentrations. (For interpretation of the references to colour in this figure legend, the reader is referred to the web version of this article.)

measurements, the carbonate leachates are clearly dominated by authigenic components, with $\delta^{234}U$ values (145 ± 7‰; 1SD, Fig. 2b) close to modern seawater, and within the range measured in well-preserved fossilised coral skeletons (Henderson and Anderson, 2003). These samples do not appear to be significantly affected by early diagenetic ^{234}U enrichment during authigenic carbonate precipitation or recrystallization (Maher et al., 2006). Similarly, the leachates do not appear to be significantly affected by the preferential leaching of ^{234}U from detrital phases during sample treatment, which would also elevate $\delta^{234}U_{CAU}$.

Systematic behaviour can also be seen for $\delta^{238}U_{bulk}$ in sapropelic samples (Fig. 2c), where the most U enriched samples have the highest $\delta^{238}U_{bulk}$, and samples with the lowest U concentrations have $\delta^{238}U_{bulk}$ similar to detrital components of modern pelagic sediments (-0.32 ± 0.06‰; 1SD; Andersen et al., 2016) and the UCC (-0.29 ± 0.03‰; Tissot & Dauphas 2015). Taken together, the relationships between both the $\delta^{234}U_{bulk}$, $\delta^{238}U_{bulk}$ and U concentrations indicate the preferential enrichment of ^{238}U in authigenic U (IV) phases and suggest that the spread in $\delta^{238}U$ of the bulk measurements is largely a result of progressive U(IV)

accumulation (i.e., defining a mixing trend between detrital and authigenic components). The $\delta^{238}U_{CAU}$ show a similar relationship as a function of U concentrations (Fig. 2d), reflecting the addition of U(IV) to the carbonate phase. However, rather than a detrital endmember, post-S1 samples with the lowest U concentrations and deposited under oxic conditions, record $\delta^{238}U_{CAU}$ values similar to seawater (−0.39‰; Andersen et al., 2017). Carbonate bound U (reflecting seawater) might also make a significant contribution to the bulk measurements in post-S1 samples, which have similar $\delta^{238}U_{bulk}$ (~-0.37‰) despite variable U concentrations (Fig. 2c) and $\delta^{234}U_{bulk}$ that are also slightly higher than secular equilibrium (+6 to + 16‰). Whilst most of the samples conform to consistent linear relationships between $\delta^{238}U_{bulk}$ and 1/U, or $\delta^{238}U_{CAU}$ and Ca/U, pre-S1 samples depart from this main trend (Fig. 2c & d), with lower $\delta^{238}U_{bulk}$ for a given U concentration (plotting on a flatter array in Fig. 2c & d). Samples from the S1-onset have higher $\delta^{238}U$ for their U concentration (defining a steeper array in Fig. 2c & d). These trends likely reflect different U reduction regimes and authigenic $\delta^{238}U$ signatures (discussed in further detail in Section 4.3).

4.2. Relationship between carbonate and bulk measurements

The above discussion indicates that $\delta^{238}U_{bulk}$ in sapropelic samples is strongly controlled by the mixing of detrital U and authigenic U(IV), suggesting that detrital contributions might explain the differences between the $\delta^{238}U_{CAU}$ and $\delta^{238}U_{bulk}$ records. To better understand the relationship between the two records we calculate $\delta^{238}U_{auth}$ from the bulk measurements by subtracting detrital contributions. Firstly, we estimate the relative proportion of authigenic U (F_{auth}) using $\delta^{234}U$ (Eq. (3); Table 3) and, for comparison, using Al concentrations (Eq. (4); Table 3). The Al-based estimates have the benefit of avoiding any issues with diagenetic ^{234}U mobilization and uncertainty in the detrital $\delta^{234}U$ (Andersen et al., 2016). Moreover, this approach is widely used in sediments that are older than the half-life of ^{234}U (Tribovillard et al., 2006). There is, however, additional uncertainty in Al-based estimates due to the large range of detrital U/Al on a global scale, reflecting both variation in source compositions and the potential for the preferential loss of U during weathering and transport (Tribovillard et al., 2006; Carpentier et al., 2013; Cole et al., 2017). Given these limitations, it is useful to compare the two approaches.

$$F_{auth-234U} = (\delta^{234}U_{bulk} - \delta^{234}U_{detrital})/(\delta^{234}U_{auth.} - \delta^{234}U_{detrital}) \qquad (3)$$

$$F_{auth-Al} = 1 - ((U/Al_{detrital} * [Al]_{bulk})/[U]_{bulk}) \qquad (4)$$

For all calculations we use a Monte Carlo approach to propagate uncertainties, reporting the mean and 2SD of the result, which uses 1000 randomly generated input variables (for $\delta^{234}U_{detrital}$ and $U/Al_{detrital}$), assuming a uniform distribution. In Eq. (3) $\delta^{234}U_{detrital}$ is assumed to be between $-20‰$ and $-9‰$ (allowing for some diagenetic loss of ^{234}U as shown for sample 40.5 cm), and $\delta^{234}U_{auth}$ is constrained by modern seawater at $146‰$. For Al-based calculations in Eq. (4) we estimate a regional detrital composition by examining the relationship of [U] *vs* [Al] in low U-concentration bulk measurements (post-sapropel and re-oxidized samples; Fig. 3). In Fig. 3, these samples define a lower detrital U/Al baseline, with a slope between $\sim$0.24 and 0.29 (ppm/wt%), which we here use as the range of $U/Al_{detrital}$. Whilst this value is significantly higher than the commonly used Post Archaean Australian Shale (PAAS; 0.11), and closer to the UCC (0.35), relatively high detrital U concentrations are also supported by Th/U values of 3.75–4.46 (ppm/ppm) in low $\delta^{234}U$ samples (Table 1), similar to the UCC (3.75; Tribovillard et al., 2006).

Using these F_{auth} estimates, we then calculate $\delta^{238}U_{auth}$ values from the bulk measurement (Table 3) by subtracting the detrital contribution (Eq. (5)) and compare these estimates with the measured $\delta^{238}U_{CAU}$ in Fig. 4. There is, however, large uncertainty associated with authigenic estimates in sediments with low U enrichments, which scales with the relative contribution of detrital material. We calculate $\delta^{238}U_{auth}$ (Eq. (5)) and propagated uncertainty (2SD) using F_{auth} derived above from both [Al] and $\delta^{234}U$ using a Monte Carlo approach. The $\delta^{238}U_{detrital}$ composition is characterized by the most detrital-rich sample (pre-S1;

40.5 cm) at $-0.34 \pm 0.07‰$ and we assume a normal distribution for uncertainty of $\delta^{238}U_{detrital}$ and $\delta^{238}U_{bulk}$.

$$\delta^{238}U_{auth} = (\delta^{238}U_{bulk} - (\delta^{238}U_{detrital} \times (1 - F_{auth})))/F_{auth} \qquad (5)$$

There is generally good agreement between $\delta^{238}U_{auth}$ and $\delta^{238}U_{CAU}$ for sapropelic samples, using both the $\delta^{234}U$- and Al-based methods (Fig. 4), suggesting that the carbonate leachates record the same $\delta^{238}U$ signature as the authigenic fraction of the bulk sediment. Pre-S1 samples also agree, but the errors for the $\delta^{238}U_{auth}$ estimates are significantly larger for these samples because of larger relative detrital fractions. For post-S1 samples, the agreement partly reflects the similarity of seawater (captured by the carbonate fraction) and detrital $\delta^{238}U$ signatures. Clear discrepancies are seen, however, between the Al-based and $\delta^{234}U$-based estimates in three of the re-oxidized samples, where the Al-based estimates give higher $\delta^{238}U_{auth}$ and are associated with significantly larger errors, while $\delta^{234}U$-based estimates better match $\delta^{238}U_{CAU}$. This likely indicates an over-estimation of the detrital contributions based on [Al] for these samples and would point to a more U-depleted detrital endmember compared to the regional estimate, for the same $\delta^{238}U_{detrital}$ composition. A lower than assumed $\delta^{238}U_{detrital}$ could also create higher $\delta^{238}U_{auth}$ estimates, but this would not explain the larger error of these samples, which derives from larger relative detrital contributions. A better agreement between the two $\delta^{238}U_{auth}$ calculations, and with $\delta^{238}U_{CAU}$, requires $U/Al_{detrital}$ of $\sim$0.2 (ppm/wt%). This is only $\sim$20% lower than the regional estimate, highlighting the problems of relying on Al-based detrital corrections for $\delta^{238}U_{auth}$ estimates in samples with low U enrichments.

Considering the above, comparison of calculated $\delta^{238}U_{auth}$ with $\delta^{238}U_{CAU}$ demonstrates that the carbonate phases record the same, first-order, redox dependant U isotope enrichments as bulk authigenic phases. Thus, the striking differences between the $\delta^{238}U_{bulk}$ and $\delta^{238}U_{CAU}$ records in Fig. 1 can largely be explained as a function of detrital contributions to bulk measurements. This relationship can also be seen by comparing $\delta^{238}U$ for the two fractions as a function of $\delta^{234}U$ (Fig. 5a). All $\delta^{238}U_{CAU}$ (circles in Fig. 5a) are associated with $\delta^{234}U_{CAU}$ close to modern seawater, whilst the respective bulk measurements (diamonds in Fig. 5a) all have lower $\delta^{234}U_{bulk}$, closer to secular equilibrium. Interpolation between the carbonate and bulk measurements in $\delta^{234}U$ – $\delta^{238}U$ space (Fig. 5a), and extrapolation of this trend, demonstrates a common convergence point for most samples, which is consistent with typical $\delta^{238}U_{detrital}$ and $\delta^{234}U_{detrital}$ compositions, and similar to the measured pre-S1 sample with lowest $\delta^{234}U_{bulk}$ and U concentration. The two samples at the onset of S1 (black symbols, Fig. 5a) imply a lower $\delta^{238}U_{detrital}$, although extrapolation is clearly more uncertain for these two samples where the fractions have more similar $\delta^{234}U$ values, and a better agreement can be seen with the rest of the samples when the error bars are considered. Notably, the bulk digest measurements for the samples that suffered re-oxidation plot at lower $\delta^{238}U_{bulk}$ and $\delta^{234}U_{bulk}$ com-

Table 3
Calculated authigenic values for bulk digests and simulated bulk compositions assuming $\delta^{238}U_{CAU}$ as the authigenic end member.

| Zone	Total Depth (cm)	Age (kyrs)	δ^{234}U-based						U/Al-based					
			F_{auth}	U_{auth} (ppm)	$\delta^{238}U_{auth}$ (‰)	2SD	$\delta^{238}U_{bulk\text{-}simulated}$ (‰)	2SD	F_{auth}	U_{auth} (ppm)	$\delta^{238}U_{auth}$ (‰)	2SD	$\delta^{238}U_{bulk\text{-}simulated}$ (‰)	2SD
Post S1	1.50	0.458	0.13	0.18	−0.80	0.52	−0.34	0.06	0.26	0.37	−0.57	0.22	−0.35	0.06
Post S1	5.50	1.678	0.18	0.22	−0.56	0.33	−0.35	0.06	0.22	0.26	−0.52	0.28	−0.35	0.06
Post S1	9.50	2.898	0.21	0.25	−0.39	0.26	−0.35	0.06	0.18	0.22	−0.40	0.34	−0.35	0.06
Post S1	13.50	4.118	0.18	0.23	−0.57	0.34	−0.35	0.06	0.39	0.52	−0.44	0.11	−0.36	0.05
Post S1	16.50	5.033	0.18	0.24	−0.44	0.31	−0.33	0.06	0.39	0.51	−0.39	0.11	−0.33	0.05
S1 termination	19.50	5.948	0.18	0.26	−0.29	0.33	−0.29	0.06	0.20	0.28	−0.29	0.31	−0.28	0.06
S1 termination	20.50	6.231	0.22	0.32	−0.12	0.24	−0.28	0.06	0.34	0.49	−0.19	0.14	−0.24	0.06
S1 oxidized	22.50	6.756	0.25	0.40	0.22	0.22	−0.21	0.06	0.10	0.16	1.57	2.95	−0.29	0.08
S1 oxidized	23.50	7.019	ND	ND	ND	ND	ND	ND	ND	ND	ND	ND	ND	ND
S1 oxidized	24.50	7.281	0.36	0.60	0.21	0.13	−0.10	0.06	0.15	0.25	1.10	1.05	−0.24	0.08
S1 oxidized	26.50	7.806	0.42	0.84	0.26	0.10	−0.09	0.05	0.43	0.85	0.25	0.13	−0.09	0.06
S1 oxidized	28.50	8.331	0.43	0.80	0.19	0.10	−0.12	0.05	0.23	0.43	0.67	0.44	−0.22	0.07
S1 residual	29.50	8.594	0.58	1.79	0.26	0.05	0.04	0.05	0.55	1.69	0.30	0.08	0.02	0.06
S1 residual	30.50	8.856	0.63	1.97	0.29	0.04	0.04	0.06	0.76	2.37	0.19	0.03	0.12	0.06
S1 residual	31.50	9.119	0.66	2.56	0.39	0.04	0.13	0.06	0.61	2.38	0.45	0.07	0.10	0.06
S1 residual	32.50	9.381	0.80	6.53	0.40	0.02	0.22	0.06	0.86	7.05	0.34	0.02	0.26	0.07
S1 onset	33.75	9.775	0.83	6.65	0.63	0.02	0.51	0.07	0.82	6.61	0.64	0.03	0.50	0.07
S1 onset	36.00	10.207	0.82	7.02	0.48	0.02	0.36	0.07	0.90	7.67	0.41	0.01	0.43	0.07
Pre S1	38.00	10.978	0.20	0.37	−0.45	0.28	−0.31	0.06	0.61	1.12	−0.37	0.05	−0.27	0.06
Pre S1	40.00	11.775	0.03	0.05	−0.26	42.03	−0.34	0.07	0.34	0.46	−0.34	0.14	−0.29	0.05

ND = not determined.
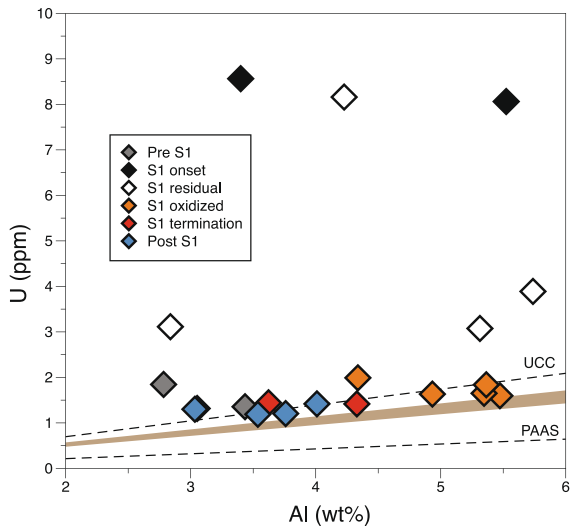
Fig. 3. U *vs.* Al plot used to estimate a range of regional detrital U/Al compositions. Shaded area represents the best estimate of regional detrital U/Al. The detrital compositions for UCC and PAAS are shown for comparison (dashed lines). Using PAAS to define the detrital contribution would result in an overestimate of authigenic uranium whereas using UCC would underestimate it.

pared to both their equivalent $\delta^{238}U_{CAU}$ and the S1-residual samples (Fig. 5a), but the extrapolation line with the respective $\delta^{238}U_{CAU}$ still defines a mixing line that passes through the likely detrital endmember (Fig. 5a). From this we suggest that any post-depositional oxidative liberation of authigenic U(IV) was not associated with significant isotope fractionation, consistent with published oxidation experiments (Wang et al., 2015). Rather, these samples mainly show a greater relative contribution of detrital U due to authigenic U(IV) loss. With this hypothe-

sized open-system U loss, there is also no reason to invoke secondary adsorption of isotopically light U onto Fe-Mn oxides or residual solid phases in the re-oxidized interval (Wang et al., 2015) which could also drive $\delta^{238}U_{bulk}$ to lower values than $\delta^{238}U_{CAU.}$

As an alternative way to quantitatively assess the identified mixing relationship, we simulate $\delta^{238}U_{bulk}$ per sample ($\delta^{238}U_{bulk-simulated}$), assuming that $\delta^{238}U_{CAU}$ is representative of the authigenic component, and compare this to the measured $\delta^{238}U_{bulk}$:

$$\delta^{238}U_{bulk-simulated} = ((1 - F_{auth}) * \delta^{238}U_{detrital})$$
$$+ (F_{auth} * \delta^{238}U_{CAU}) \qquad (6)$$

Again, we use a Monte Carlo approach to calculate the mean $\delta^{238}U_{bulk-simulated}$ and associated error (2SD). For all samples there is excellent agreement between the simulated and measured $\delta^{238}U_{bulk}$ when using either $\delta^{234}U$ or the Al-based F_{auth} estimates ($r^2 > 0.95$), with all data within error of the 1:1 line (Fig. 5).

Whilst we assume that the ammonium acetate leachates exclusively liberate carbonate bound U, the consistency of $\delta^{238}U_{CAU}$ and $\delta^{238}U_{auth}$ could plausibly reflect the oxidative mobilization of non-carbonate reduced U phases (i.e. bulk authigenic U(IV)) during leaching. Whilst we cannot rule this possibility out, we note that abundant U(IV) in carbonate is consistent with several published observations. Firstly, U/Ca in picked foraminifera is known to semi-quantitatively track total authigenic U enrichments due to the accumulation of U(IV) in authigenic carbonate cements and coatings (Boiteau et al., 2012; Gottschalk et al., 2016). Secondly, U(IV), with a similar ionic radius to Ca^{2+}, is readily substituted into the calcite lattice (Sturchio et al., 1998; Zhao et al., 2016) in contrast to U(VI) which must undergo a coordination change (Reeder et al., 2001). Additionally, with the tight coupling of authigenic carbonate
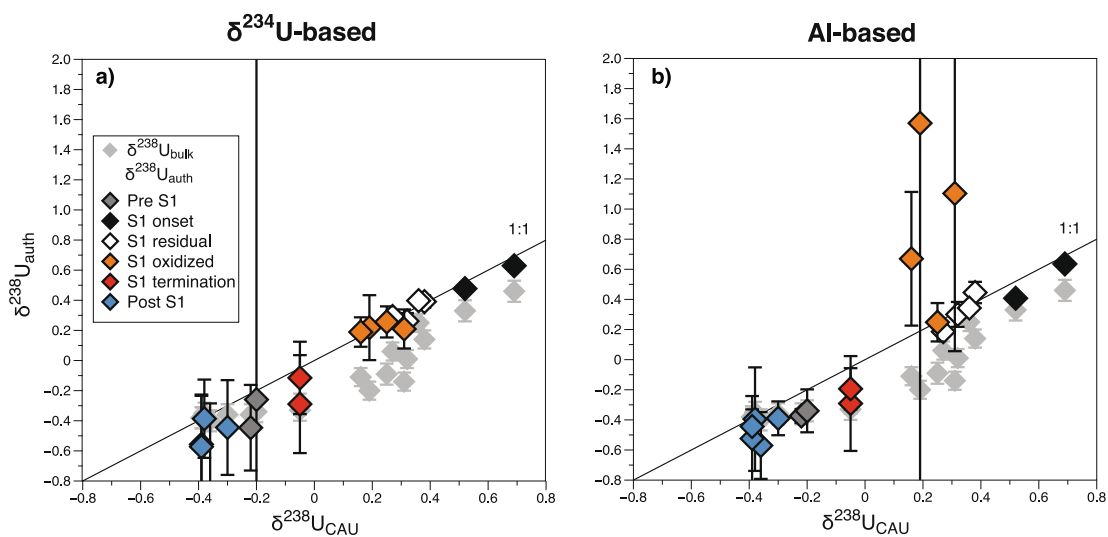

Fig. 4. Comparison of calculated $\delta^{238}U_{auth}$ and $\delta^{238}U_{CAU}$. (a) $\delta^{234}U$-based authigenic estimates and (b) U/Al-based. For comparison, $\delta^{238}U_{bulk}$ are shown as shaded symbols. Error estimates for $\delta^{238}U_{auth}$ incorporate uncertainty of the $\delta^{238}U_{detital}$ and $\delta^{234}U_{detrital}$ endmembers, and the uncertainty of regional detrital U/Al. The Al-based estimates clearly result in an overcorrection compared to the $\delta^{234}U$ derived estimates for the re-oxidized samples, and sometimes very large uncertainties.
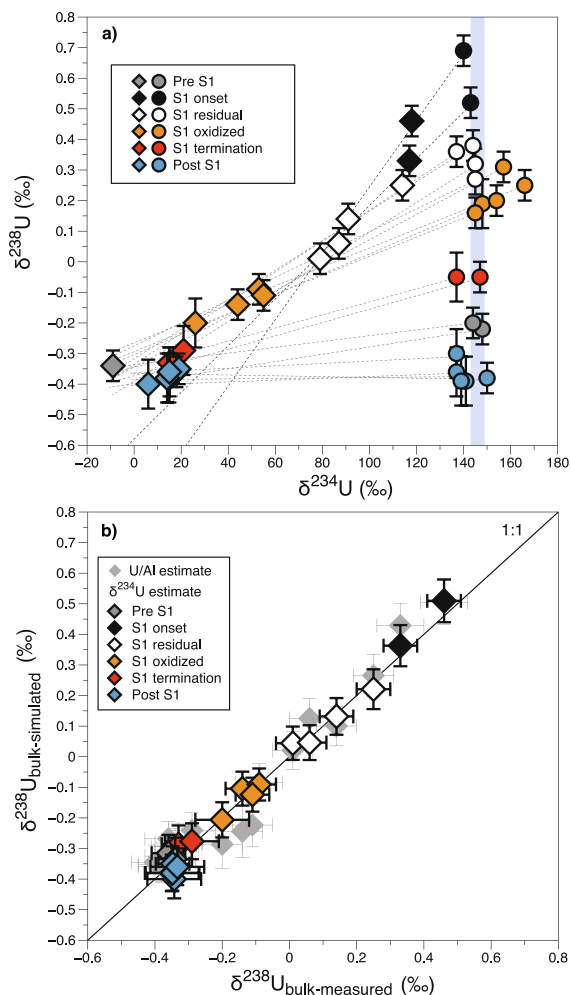
Fig. 5. Quantitative assessment of detrital mixing as a control on $\delta^{238}U_{bulk}$. (a) Comparison of measured carbonate (circles) and bulk (diamonds) $\delta^{238}U$ for each sample as a function of $\delta^{234}U$, demonstrating a mixing relationship between authigenic and detrital signatures. (b) Plot of simulated $\delta^{238}U_{bulk}$ against measured $\delta^{238}U_{bulk}$, used to quantitatively assess how well the data can be explained by a simple mixing model between a detrital endmember and an authigenic endmember that is recorded by the carbonate fraction.

precipitation and U reduction, due to alkalinity generation from sulfate reduction, disproportionately large U enrichments (ppm level) are expected in authigenic calcite under reducing conditions (Zhao et al., 2016). Indeed, in-situ measurements of diagenetically altered foraminiferal specimens, from zones of active sulfate reduction and anaerobic methane oxidation, have U/Ca up to ~34 μmol/mol (Detlef et al., 2020), meaning that the high U/Ca of the ammonium acetate leachates in sapropelic samples (0.5–9.4 μmol/mol; Table 2) can be readily explained as reflecting carbonate bound U(IV) without invoking the oxidative liberation of other reduced U phases. Dedicated leaching tests are required to address this question, but, regardless of the precise mineralogical phase that is leached with buffered ammonium acetate, the leaching technique

successfully isolates the authigenic U(IV) component in sapropelic samples.

The above discussion therefore demonstrates that i) the carbonate leachates predominantly record authigenic $\delta^{234}U$ and $\delta^{238}U$ values and ii) bulk $\delta^{238}U$ data are consistent with a mixture between this authigenic value and a detrital end-member. Thus, $\delta^{238}U_{CAU}$ can be used to reconstruct local redox changes in the same manner as $\delta^{238}U_{auth}$, but avoids the uncertainty associated with detrital corrections in low-U enrichment (or diagenetically oxidized) sediments.

4.3. Comparison to Site 967

For further insights into the preservation of authigenic $\delta^{238}U$ values we compare the 64PE406-E1 data to the nearby ODP Site 967 (Fig. 6). Site 967 is situated at a greater depth (2252 m) in the Eastern Mediterranean, one that was characterized by lower ventilation rates during S1 (De Lange et al., 2008). As such, Site 967 generally shows greater U enrichments and, whilst there is a Mn peak associated with the later return to oxic conditions at the top of the sapropel, redox sensitive metals and TOC remain elevated throughout S1, with no strong evidence for diagenetic redistribution or secondary immobilization of U (Azrieli-Tal et al., 2014; Andersen et al., 2020). Site 967 also records the same distinctive double Ba/Al peak (Grant et al., 2017; Andersen et al., 2020) as seen at 64PE406-E1, used here for age correlation (Fig. 6; see Section 2). For temporal comparisons of authigenic $\delta^{238}U$ values between the sites, we use Al-based estimates from Site 967 (after Andersen et al., 2020) and $\delta^{234}U$-based estimates for site 64PE406-E1 (which appear to be more accurate in this case), in addition to $\delta^{238}U_{CAU}$ (Fig. 6). We also examine trends in $\delta^{238}U_{auth}$ for Site 967 as a function of authigenic U concentrations (U_{auth}), and both $\delta^{238}U_{auth}$ and $\delta^{238}U_{CAU}$ for site 64PE406-E1 (Fig. 7).

A first-order comparison of the two sites (Fig. 6) demonstrates broad agreement of $\delta^{238}U$ through S1, despite the clear loss of authigenic U in the upper half of S1 at Site 64PE406-E1. These patterns confirm that $\delta^{238}U_{auth}$ and $\delta^{238}U_{CAU}$ have not been significantly compromised by oxidative diagenesis, although U concentrations clearly have (Fig. 6b). This can also be seen in $1/U_{auth} - \delta^{238}U_{auth}$ space (Fig. 7a). Fig. 7 shows that all the data for Site 64PE406-E1 have lower U_{auth} than Site 967, reflecting lower U accumulation rates. But samples from the re-oxidized and sapropel termination intervals have even lower U_{auth} for similar $\delta^{238}U_{auth}$, defining horizontal arrays that are indicative of oxidative U loss, in contrast to the linear trend formed by the Site 967 data (Fig. 7a). Whilst we can calculate $\delta^{238}U_{auth}$, and the current concentration of U_{auth} in the sample, we cannot know how much U has been lost and, therefore, cannot reconstruct primary U_{auth} enrichments. It is also noteworthy that in $\delta^{238}U_{CAU} - Ca/U$ space (Fig. 7b) the carbonate measurements from the re-oxidized interval also show slightly elevated $\delta^{238}U_{CAU}$ values, being outside of the 95% confidence interval of the main linear regression (Fig. 2d). Importantly, if this were the result of the secondary immobilization of diagenetically liberated U(IV) we would expect the samples to follow the
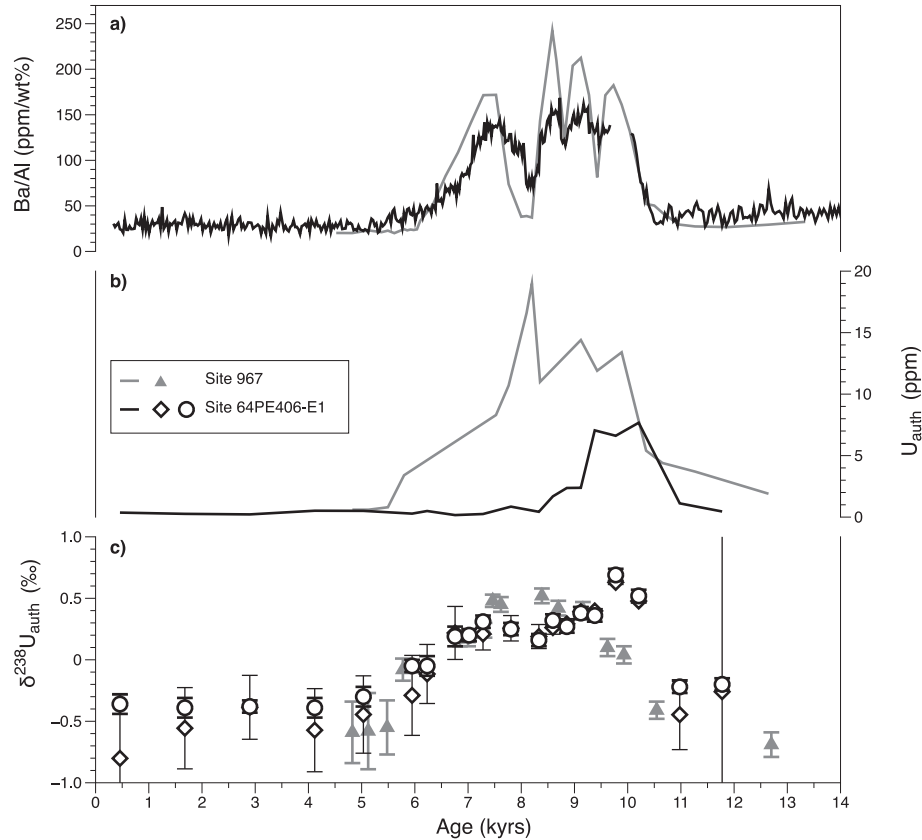
Fig. 6. Comparison of temporal trends in U systematics for Site 64PE406-E1 and Site 967. (a) Ba/Al for Sites 967 (grey line; Andersen et al., 2020) and 64PE406-E1 (black line), used for temporal correlation of the two sites. (b) Authigenic U concentrations for Sites 967 (grey line; Andersen et al., 2020) and 64PE406-E1 (black line), showing the clear loss of U at the shallower site during the upper part of S1. (c) $\delta^{238}U_{auth}$ for Site 967 (grey triangles; Andersen et al, 2020) as well as both $\delta^{238}U_{auth}$ (open diamonds) and $\delta^{238}U_{CAU}$ (open circles) for Site 64PE406-E1. $\delta^{238}U$ trends show clear similarities throughout S1, suggesting that carbonate bound U records the same authigenic signatures recorded in bulk sediments. But the carbonate phase retains this isotopic signature during subsequent oxidative diagenesis, where bulk authigenic U is removed. $\delta^{238}U_{CAU}$ from samples after S1 show seawater values, whereas bulk measurements are dominated by detrital contributions, leading to larger errors.

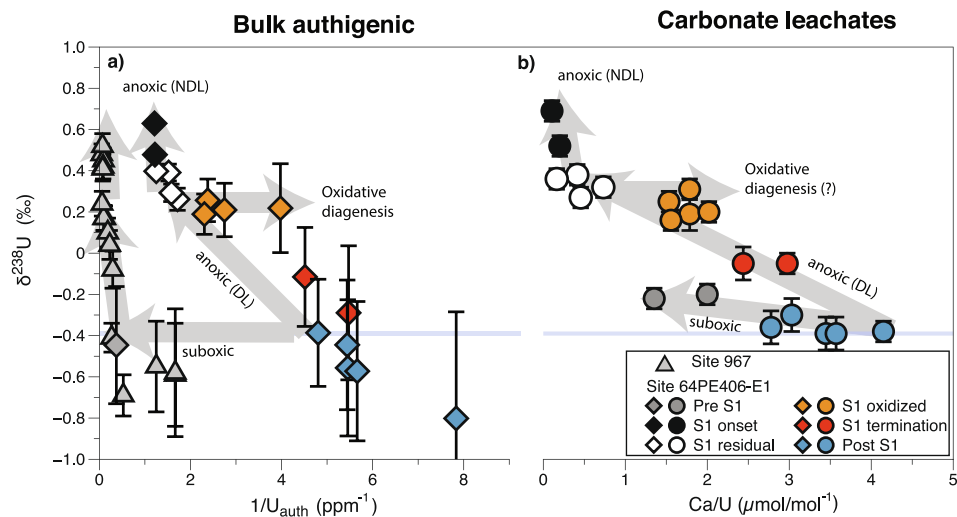Fig. 7. Comparison of U systematics for Site 64PE406-E1 and Site 967. (a) $\delta^{238}U_{auth}$ estimates for Site 967 and 64PE406-E1 for samples with uncertainty <1‰, as a function of authigenic U concentrations (b) $\delta^{238}U_{CAU}$ for Site 64PE406-E1 that are thought to be representative of $\delta^{238}U_{auth}$. DL = diffusion limited, NDL = non-diffusion limited.

same trend as the rest of the data, with both increasing U concentrations and $\delta^{238}U_{CAU}$. The observed profile might instead suggest that the carbonate phase has also suffered the diagenetic loss of U during oxidation (resulting in lower [U] for the same $\delta^{238}U_{CAU}$), or it may be an artefact related to the uncertainty in defining the U concentrations of the oxic endmember, as there can be multiple controls on U/Ca in oxic bulk carbonates (see Clarkson et al., 2021).

In pre-S1 samples, $\delta^{238}U_{CAU}$ at 64PE406-E1 are similar to modern hypoxic to suboxic localities (Weyer et al., 2008; Andersen et al., 2016), which is in accordance with the inferred deglaciation-driven prelude to deep-water stagnation (Grimm et al., 2015) and higher Ba/Al than post-S1 samples (Fig. 1). These samples plot on a flatter array in Ca/U – $\delta^{238}U_{CAU}$ space (Fig. 7b), with moderate U enrichments in the carbonate phase for a minor increase in $\delta^{238}U_{CAU}$; a trend that is distinct from the rest of the S1 samples. The $\delta^{238}U_{CAU}$ therefore appears to sensitively capture redox variations before the initiation of S1, whilst $\delta^{238}U_{auth}$ at both sites is not resolvable from detrital values (Fig. 6).

Whilst both localities show similarly high $\delta^{238}U_{auth}$ values through S1, there are notable differences in places. In particular, at the very onset of S1, 64PE406-E1 records an earlier and higher $\delta^{238}U_{auth}$ maximum, reaching values up to ~1.1‰ above seawater (Fig. 6) and close to the suggested full U isotope enrichment factor (~1.2‰; Andersen et al., 2014; Basu et al., 2014; Stirling et al., 2015; Brown et al., 2018). These elevated $\delta^{238}U$ compositions define a steeper trajectory in Ca/U – $\delta^{238}U_{CAU}$ and $1/U_{auth}$ – $\delta^{238}U_{auth}$ space (Fig. 7), with higher $\delta^{238}U$ values for any given concentration, that separates the samples from the rest of the dataset. Importantly, this characteristic is also seen in the $\delta^{238}U_{auth}$ data for Site 967 (Fig. 7a), suggesting that this trend is likely a primary feature that reflects a change in the reducing environment and U isotope fractionation factor, relative to the rest of the samples, and is not an artefact of oxidative diagenesis at Site 64PE406-E1. Because U reduction predominantly occurs at or below the sediment–water interface, one model to explain variable $\delta^{238}U_{auth}$ focusses on the diffusion constraints on U transport and precipitation (Clark and Johnson, 2008; Andersen et al., 2014). In diffusion limited (DL) regimes, the expected isotope enrichment is up to half (+0.6‰) the suggested full isotope enrichment factor (~1.2‰; Andersen et al., 2014; Basu et al., 2014; Stirling et al., 2015; Brown et al., 2018). Isotope enrichments above this can be caused by DL reduction with non-quantitative U removal (Andersen et al., 2014), resulting in lower total U enrichments, or in situations where there is non-diffusion limited (NDL) reduction at the sediment–water interface (Andersen et al., 2017). Such NDL reduction might be linked to the development of an organic rich flocule layer, previously proposed to explain high $\delta^{238}U_{auth}$ values for S1 at Site 967 (Andersen et al., 2020) and consistent with previous interpretations of an 'anoxic blanket' restricted to the seafloor during S1 as a result of high organic carbon delivery (Casford et al., 2003). The fact that $\delta^{238}U_{auth}$ and $\delta^{238}U_{CAU}$ are higher at Site 64PE406-E1 during the onset of S1 likely indicates a greater expression of NDL reduction, whereas Site 967

experienced more extensive U_{auth} enrichments under more reducing, or more temporally stable, conditions but with greater diffusion limitation. Nevertheless, this balance in reduction regime apparently changed later in S1, when a stronger expression of NDL reduction can be seen at Site 967. More significant NDL contributions could also explain the slight elevation in $\delta^{238}U_{CAU}$ for a given Ca/U in the re-oxidized samples (Fig. 7b), rather than invoking the diagenetic loss of U from the carbonate phase as discussed above.

Throughout S1 there is an excellent correspondence between Ba/Al and $\delta^{238}U_{CAU}$ (Fig. 1) for Site 64PE406-E1. This is consistent with authigenic U(IV) enrichment that was proximally driven by O_2 depletion because of heightened productivity, organic carbon supply and aerobic remineralisation, whilst the more stratified water-column simultaneously reduced the oxygen supply to the deep sea (Casford et al., 2003; Rohling et al., 2015). The detailed structure of the $\delta^{238}U_{CAU}$ and Ba/Al records also identifies short term fluctuations, including the often-observed sapropel interruption at ~8.5–7.8 cal. kyr BP and even more minor (centennial scale) variance. This proxy coupling is partly seen at Site 967, although the sapropel interruption is not as clearly recorded in U systematics (Azrieli-Tal et al., 2014; Andersen et al., 2020), likely a limitation of sample resolution.

4.4. Implications for reconstructing seawater $\delta^{238}U$

To date, most applications of carbonate $\delta^{238}U$ have sought to reconstruct open ocean $\delta^{238}U$ to identify the expansion of benthic anoxia on a global scale (see Zhang et al., 2020). The post-S1 samples, that were deposited under oxygenated conditions, support the use of pelagic carbonates as an archive in this manner (see also Clarkson et al., 2018; Tissot et al., 2018; del Rey et al., 2020; Clarkson et al., 2021). The U/Ca of post-S1 carbonate leachates are higher than expected for biogenic calcite (e.g. foraminifera), and likely reflect U incorporation into abiotic cements, but appear to passively record seawater $\delta^{238}U$ values. Some pelagic carbonates, however, record $\delta^{238}U_{CAU}$ that are lower than seawater (Clarkson et al., 2020; Clarkson et al., 2021), possibly due to the role of adsorption during co-precipitation, but the specific environmental controls on these $\delta^{238}U$ signatures requires further investigation. It seems that, at least in some cases, seawater $\delta^{238}U$ signatures can be preserved in ancient calcite sediments, with no significant modification as the sediment passes through anoxic diagenetic zones. This is likely related to large oxygen penetration depths that limit U diffusion to deeper diagenetic zones, but further research is required on this.

As the chemocline shoals and, in the case of the sapropels, reaches bottom waters, authigenic U(IV) addition to carbonates overwhelms primary seawater $\delta^{238}U$ signatures, expanding the application of $\delta^{238}U_{CAU}$ as a local indicator of anoxia in pelagic settings. But this will also lead to complications for interpreting carbonate records in terms of global changes in seawater $\delta^{238}U$, so that complementary information on benthic oxygenation will be required to

reconstruct seawater $\delta^{238}U$. The simple combination of U/Ca and $\delta^{238}U$ might provide a useful framework for identifying anoxic samples, as the two are clearly coupled in anoxic calcite-rich sediments (see also Clarkson et al., 2021) and this relationship is largely preserved during oxidative diagenesis. For this purpose, acetic based leachates (preferably pH buffered) are essential for avoiding detrital U, which can lead to higher U/Ca values with little effect on $\delta^{238}U$, obscuring clear trends indicative of de-oxygenation (Clarkson et al., 2020). The more variable U concentrations of mixed mineralogy carbonates from shallow-water settings, however, would complicate these straightforward relationships, as would secular changes in seawater $\delta^{238}U$ during global carbon cycle perturbations. Support for global trends in seawater $\delta^{238}U$ should always come from multiple sections and careful integration with multiple geochemical and palaeontological datasets. An example of this approach is represented by the Paleocene Eocene Thermal Maximum, where foraminiferal data, Ce-anomaly and Cr isotopes provide support for the interpretation of local de-oxygenation that can clearly be seen in U/Ca and $\delta^{238}U_{CAU}$ (Clarkson et al., 2021). There also appears to be some threshold of U/Ca where $\delta^{238}U_{CAU}$ is significantly modified (Clarkson et al., 2021), although this precise point is unlikely to be universal.

5. CONCLUSION

Sapropelic samples demonstrate that the carbonate phases record similar isotope compositions to bulk authigenic U(IV) phases, but there is significantly less uncertainty associated with $\delta^{238}U_{CAU}$, compared to $\delta^{238}U_{auth}$, due to the avoidance of detrital phases. A regional estimate of detrital compositions is clearly important for paleo-redox reconstructions using $\delta^{238}U_{auth}$ (see also Tribovillard et al., 2006; Cole et al., 2017). But, even in cases where this is relatively well constrained, $\delta^{238}U_{auth}$ is still susceptible to poor accuracy and precision in samples with low U enrichment. For sediments with higher U enrichments (e.g., Sapropel S1-onset and Site 967) the uncertainty on the detrital contribution is less important. This uncertainty can be avoided by using $\delta^{238}U_{CAU}$, which is especially useful in settings at the less extreme end of the redox spectrum, where conditions temporally fluctuate, or where post-depositional oxidative diagenesis is significant. Moreover, carbonate leachates avoid other phases that contribute U to bulk isotopic signatures but are difficult to correct for, such as isotopically light U associated with organic matter or Fe-Mn oxides, and that can mask redox dependant isotope fractionation (Brennecka et al., 2011; Holmden et al., 2015; Hinojosa et al., 2016; Abshire et al., 2020; Chen et al., 2020). Similarly, carbonate leachates largely avoid phosphate phases (Dahl et al., 2017), which could contribute significantly to the total U pool of a sample but may have $\delta^{238}U$ signatures that are closer to seawater. Thus, we suggest that $\delta^{238}U_{CAU}$ can be a useful tool for reconstructing redox conditions in ancient sediments, and for better understanding the controls on isotope fractionation in low U-enrichment settings. Importantly, this study also demonstrates that the authigenic $\delta^{238}U$ sig-natures (bulk and carbonate) are not significantly affected by post-depositional oxidation, so that they can be used to reliably reconstruct benthic redox changes despite the later return to oxygenated conditions. Care must still be taken, however, to identify secondary U enrichments in sediments, caused by oxidative liberation and re-precipitation under reducing conditions deeper in the sediment (Mangini et al., 2001).

Finally, whilst this study focuses on the behaviour of U in carbonates in reducing settings, post-S1 samples, deposited under oxic conditions, add to the growing body of literature that supports the use of pelagic, calcite-rich sediments as a reliable paleo-archive of seawater signatures (Clarkson et al., 2018; Tissot et al., 2018; del Rey et al., 2020; Clarkson et al., 2021). We therefore confirm that pelagic carbonate $\delta^{238}U$ can be a versatile tool for characterising trends in open-ocean seawater $\delta^{238}U$, related to the global-scale expansion of benthic anoxia. Here, we also propose their novel application to local reconstructions of benthic redox conditions.

Declaration of Competing Interest

The authors declare that they have no known competing financial interests or personal relationships that could have appeared to influence the work reported in this paper.

APPENDIX A. SUPPLEMENTARY MATERIAL

Supplementary data to this article can be found online at https://doi.org/10.1016/j.gca.2021.07.025.

REFERENCES

Abshire M. L., Romaniello S. J., Kuzminov A. M., Cofrancesco J., Severmann S. and Riedinger N. (2020) Uranium isotopes as a proxy for primary depositional redox conditions in organic-rich marine systems. *Earth Planet. Sci. Lett.* **529** 115878.

Abu-Zied R. H., Rohling E. J., Jorissen F. J., Fontanier C., Casford J. S. and Cooke S. (2008) Benthic foraminiferal response to changes in bottom-water oxygenation and organic carbon flux in the eastern Mediterranean during LGM to Recent times. *Mar. Micropaleontol.* **67**, 46–68.

Algeo T. J. and Liu J. (2020) A re-assessment of elemental proxies for paleoredox analysis. *Chem. Geol.* **540** 119549.

Andersen M., Matthews A., Bar-Matthews M. and Vance D. (2020) Rapid onset of ocean anoxia shown by high U and low Mo isotope compositions of sapropel S1. *Geochem. Perspect. Lett.* **15**, 10–14.

Andersen M., Romaniello S., Vance D., Little S., Herdman R. and Lyons T. (2014) A modern framework for the interpretation of $^{238}U/^{235}U$ in studies of ancient ocean redox. *Earth Planet. Sci. Lett.* **400**, 184–194.

Andersen M., Stirling C., Zimmermann B. and Halliday A. (2010) Precise determination of the open ocean $^{234}U/^{238}U$ composition. *Geochem. Geophys. Geosyst.* **11**.

Andersen M., Stirling C. H. and Weyer S. (2017) Uranium isotope fractionation. *Rev. Mineral. Geochem.* **82**, 799–850.

Andersen M., Vance D., Morford J., Bura-Nakić E., Breitenbach S. and Och L. (2016) Closing in on the marine $^{238}U/^{235}U$ budget. *Chem. Geol.* **420**, 11–22.

Azrieli-Tal I., Matthews A., Bar-Matthews M., Almogi-Labin A., Vance D., Archer C. and Teutsch N. (2014) Evidence from molybdenum and iron isotopes and molybdenum–uranium covariation for sulphidic bottom waters during Eastern Mediterranean sapropel S1 formation. *Earth Planet. Sci. Lett.* **393**, 231–242.

Bale N. J., Hennekam R., Hopmans E. C., Dorhout D., Reichart G.-J., van der Meer M., Villareal T. A., Sinninghe Damsté J. S. and Schouten S. (2019) Biomarker evidence for nitrogen-fixing cyanobacterial blooms in a brackish surface layer in the Nile River plume during sapropel deposition. *Geology* **47**, 1088–1092.

Basu A., Sanford R. A., Johnson T. M., Lundstrom C. C. and Löffler F. E. (2014) Uranium isotopic fractionation factors during U(VI) reduction by bacterial isolates. *Geochim. Cosmochim. Acta* **136**, 100–113.

Bishop J. K. (1988) The barite-opal-organic carbon association in oceanic particulate matter. *Nature* **332**, 341–343.

Boiteau R., Greaves M. and Elderfield H. (2012) Authigenic uranium in foraminiferal coatings: a proxy for ocean redox chemistry. *Paleoceanography* **27**.

Brennecka G. A., Wasylenki L. E., Bargar J. R., Weyer S. and Anbar A. D. (2011) Uranium isotope fractionation during adsorption to Mn-oxyhydroxides. *Environ. Sci. Technol.* **45**, 1370–1375.

Brown S. T., Basu A., Ding X., Christensen J. N. and DePaolo D. J. (2018) Uranium isotope fractionation by abiotic reductive precipitation. *Proc. Natl. Acad. Sci.* **115**, 8688.

Brüske A., Weyer S., Zhao M.-Y., Planavsky N., Wegwerth A., Neubert N., Dellwig O., Lau K. and Lyons T. (2020) Correlated molybdenum and uranium isotope signatures in modern anoxic sediments: implications for their use as paleoredox proxy. *Geochim. Cosmochim. Acta* **270**, 449–474.

Bura-Nakić E., Andersen M. B., Archer C., De Souza G. F., Marguš M. and Vance D. (2018) Coupled Mo-U abundances and isotopes in a small marine euxinic basin: constraints on processes in euxinic basins. *Geochim. Cosmochim. Acta* **222**, 212–229.

Canfield D. E., Raiswell R. and Bottrell S. (1992) The reactivity of sedimentary iron minerals toward sulfide. *Am. J. Sci.* **292**, 659–683.

Carpentier M., Weis D. and Chauvel C. (2013) Large U loss during weathering of upper continental crust: the sedimentary record. *Chem. Geol.* **340**, 91–104.

Casford J. S. L., Rohling E. J., Abu-Zied R. H., Fontanier C., Jorissen F. J., Leng M. J., Schmiedl G. and Thomson J. (2003) A dynamic concept for eastern Mediterranean circulation and oxygenation during sapropel formation. *Palaeogeogr. Palaeoclimatol. Palaeoecol.* **190**, 103–119.

Chen X., Romaniello S. J., Herrmann A. D., Hardisty D., Gill B. C. and Anbar A. D. (2018a) Diagenetic effects on uranium isotope fractionation in carbonate sediments from the Bahamas. *Geochim. Cosmochim. Acta* **237**, 294–311.

Chen X., Romaniello S. J., Herrmann A. D., Samankassou E. and Anbar A. D. (2018b) Biological effects on uranium isotope fractionation ($^{238}U/^{235}U$) in primary biogenic carbonates. *Geochim. Cosmochim. Acta* **240**, 1–10.

Chen X., Romaniello S. J., Herrmann A. D., Wasylenki L. E. and Anbar A. D. (2016) Uranium isotope fractionation during coprecipitation with aragonite and calcite. *Geochim. Cosmochim. Acta* **188**, 189–207.

Chen X., Romaniello S. J., McCormick M., Sherry A., Havig J. R., Zheng W. and Anbar A. D. (2021) Anoxic depositional overprinting of $^{238}U/^{235}U$ in calcite: when do carbonates tell black shale tales? *Geology* **49**.

Chen X., Zheng W. and Anbar A. D. (2020) Uranium isotope fractionation ($^{238}U/^{235}U$) during U (VI) uptake by freshwater plankton. *Environ. Sci. Technol.* **54**, 2744–2752.

Clark S. K. and Johnson T. M. (2008) Effective isotopic fractionation factors for solute removal by reactive sediments: a laboratory microcosm and slurry study. *Environ. Sci. Technol.* **42**, 7850–7855.

Clarkson M. O., Lenton T. M., Andersen M. B., Bagard M.-L., Dickson A. J. and Vance D. (2021) Upper limits on the extent of seafloor anoxia during the PETM from uranium isotopes. *Nat. Commun.* **12**, 1–9.

Clarkson M. O., Müsing K., Andersen M. B. and Vance D. (2020) Examining pelagic carbonate-rich sediments as an archive for authigenic uranium and molybdenum isotopes using reductive cleaning and leaching experiments. *Chem. Geol.* **539** 119412.

Clarkson M. O., Stirling C. H., Jenkyns H. C., Dickson A. J., Porcelli D., Moy C. M., von Strandmann P. A. P., Cooke I. R. and Lenton T. M. (2018) Uranium isotope evidence for two episodes of deoxygenation during Oceanic Anoxic Event 2. *Proc. Natl. Acad. Sci.*, 2918–2923.

Cole D. B., Zhang S. and Planavsky N. J. (2017) A new estimate of detrital redox-sensitive metal concentrations and variability in fluxes to marine sediments. *Geochim. Cosmochim. Acta* **215**, 337–353.

Dahl T. W., Connelly J., Kouchinsky A., Gill B., Månsson S. and Bizzarro M. (2017) Reorganisation of Earth's biogeochemical cycles briefly oxygenated the oceans 520 Myr ago. *Geochem. Perspect.* **3**, 210–220.

De Lange G. J., Thomson J., Reitz A., Slomp C. P., Principato M. S., Erba E. and Corselli C. (2008) Synchronous basin-wide formation and redox-controlled preservation of a Mediterranean sapropel. *Nat. Geosci.* **1**, 606–610.

De Rijk S., Hayes A. and Rohling E. (1999) Eastern Mediterranean sapropel S1 interruption: an expression of the onset of climatic deterioration around 7 ka BP. *Mar. Geol.* **153**, 337–343.

del Rey Á., Havsteen J. C., Bizzarro M. and Dahl T. W. (2020) Untangling the diagenetic history of uranium isotopes in marine carbonates: A case study tracing the δ^{238}U composition of late Silurian oceans using calcitic brachiopod shells. *Geochim. Cosmochim. Acta* **287**, 93–110.

DePaolo D. J., Maher K., Christensen J. N. and McManus J. (2006) Sediment transport time measured with U-series isotopes: results from ODP North Atlantic drift site 984. *Earth Planet. Sci. Lett.* **248**, 394–410.

Detlef H., Sosdian S. M., Kender S., Lear C. H. and Hall I. R. (2020) Multi-elemental composition of authigenic carbonates in benthic foraminifera from the eastern Bering Sea continental margin (International Ocean Discovery Program Site U1343). *Geochim. Cosmochim. Acta* **268**, 1–21.

Gottschalk J., Skinner L. C., Lippold J., Vogel H., Frank N., Jaccard S. L. and Waelbroeck C. (2016) Biological and physical controls in the Southern Ocean on past millennial-scale atmospheric CO_2 changes. *Nat. Commun.* **7**, 1–11.

Grant K., Grimm R., Mikolajewicz U., Marino G., Ziegler M. and Rohling E. (2016) The timing of Mediterranean sapropel deposition relative to insolation, sea-level and African monsoon changes. *Quat. Sci. Rev.* **140**, 125–141.

Grant K. M., Rohling E. J., Westerhold T., Zabel M., Heslop D., Konijnendijk T. and Lourens L. (2017) A 3 million year index for North African humidity/aridity and the implication of potential pan-African Humid periods. *Quat. Sci. Rev.* **171**, 100–118.

Grimm R., Maier-Reimer E., Mikolajewicz U., Schmiedl G., Müller-Navarra K., Adloff F., Grant K. M., Ziegler M., Lourens L. J. and Emeis K.-C. (2015) Late glacial initiation of Holocene eastern Mediterranean sapropel formation. *Nat. Commun.* **6**, 1–12.

Henderson G. M. and Anderson R. F. (2003) The U-series toolbox for paleoceanography. *Rev. Mineral. Geochem.* **52**, 493–531.

Hennekam R., Jilbert T., Schnetger B. and de Lange G. J. (2014) Solar forcing of Nile discharge and sapropel S1 formation in the early to middle Holocene eastern Mediterranean. *Paleoceanography* **29**, 343–356.

Hennekam R., van der Bolt B., van Nes E. H., de Lange G. J., Scheffer M. and Reichart G. J. (2020) Early-warning signals for marine anoxic events. *Geophys. Res. Lett.* **47**, e2020GL089183.

Higgs N., Thomson J., Wilson T. and Croudace I. (1994) Modification and complete removal of eastern Mediterranean sapropels by postdepositional oxidation. *Geology* **22**, 423–426.

Hinojosa J. L., Stirling C. H., Reid M. R., Moy C. M. and Wilson G. S. (2016) Trace metal cycling and $^{238}U/^{235}U$ in New Zealand's fjords: Implications for reconstructing global paleoredox conditions in organic-rich sediments. *Geochim. Cosmochim. Acta* **179**, 89–109.

Holmden C., Amini M. and Francois R. (2015) Uranium isotope fractionation in Saanich Inlet: a modern analog study of a paleoredox tracer. *Geochim. Cosmochim. Acta* **153**, 202–215.

Jacobel A., Anderson R., Jaccard S., McManus J., Pavia F. and Winckler G. (2020) Deep Pacific storage of respired carbon during the last ice age: Perspectives from bottom water oxygen reconstructions. *Quat. Sci. Rev.* **230** 106065.

Jung M., Ilmberger J., Mangini A. and Emeis K. C. (1997) Why some Mediterranean sapropels survived burn-down (and others did not). *Mar. Geol.* **141**, 51–60.

Kendall B. (2020) Recent Advances in Geochemical Paleo-Oxybarometers. *Annu. Rev. Earth Planet. Sci.* **49**.

Kendall B., Komiya T., Lyons T. W., Bates S. M., Gordon G. W., Romaniello S. J., Jiang G., Creaser R. A., Xiao S. and McFadden K. (2015) Uranium and molybdenum isotope evidence for an episode of widespread ocean oxygenation during the late Ediacaran Period. *Geochim. Cosmochim. Acta* **156**, 173–193.

Koopmans M. P., Köster J., Van Kaam-Peters H. M., Kenig F., Schouten S., Hartgers W. A., de Leeuw J. W. and Damsté J. S. S. (1996) Diagenetic and catagenetic products of isorenieratene: molecular indicators for photic zone anoxia. *Geochim. Cosmochim. Acta* **60**, 4467–4496.

Lau K. V., Lyons T. W. and Maher K. (2020) Uranium reduction and isotopic fractionation in reducing sediments: insights from reactive transport modeling. *Geochim. Cosmochim. Acta* **287**, 65–92.

Lyons T. W., Anbar A. D., Severmann S., Scott C. and Gill B. C. (2009) Tracking euxinia in the Ancient Ocean: a multiproxy perspective and proterozoic case study. *Annu. Rev. Earth Planet. Sci.* **37**, 507–534.

Maher K., Steefel C. I., DePaolo D. J. and Viani B. E. (2006) The mineral dissolution rate conundrum: Insights from reactive transport modeling of U isotopes and pore fluid chemistry in marine sediments. *Geochim. Cosmochim. Acta* **70**, 337–363.

Mangini A., Jung M. and Laukenmann S. (2001) What do we learn from peaks of uranium and of manganese in deep sea sediments? *Mar. Geol.* **177**, 63–78.

McManus J., Berelson W. M., Severmann S., Poulson R. L., Hammond D. E., Klinkhammer G. P. and Holm C. (2006) Molybdenum and uranium geochemistry in continental margin sediments: paleoproxy potential. *Geochim. Cosmochim. Acta* **70**, 4643–4662.

Mercone D., Thomson J., Abu-Zied R., Croudace I. and Rohling E. (2001) High-resolution geochemical and micropalaeontological profiling of the most recent eastern Mediterranean sapropel. *Mar. Geol.* **177**, 25–44.

Mercone D., Thomson J., Croudace I., Siani G., Paterne M. and Troelstra S. (2000) Duration of S1, the most recent sapropel in the eastern Mediterranean Sea, as indicated by accelerator mass spectrometry radiocarbon and geochemical evidence. *Paleoceanography* **15**, 336–347.

Meyer K. M. and Kump L. R. (2008) Oceanic euxinia in Earth history: Causes and consequences. *Annu. Rev. Earth Planet. Sci.* **36**, 251–288.

Montoya-Pino C., Weyer S., Anbar A. D., Pross J., Oschmann W., van de Schootbrugge B. and Arz H. W. (2010) Global enhancement of ocean anoxia during Oceanic Anoxic Event 2: a quantitative approach using U isotopes. *Geology* **38**, 315–318.

Morford J. L., Martin W. R. and Carney C. M. (2009) Uranium diagenesis in sediments underlying bottom waters with high oxygen content. *Geochim. Cosmochim. Acta* **73**, 2920–2937.

Poulton S. W., Krom M. D. and Raiswell R. (2004) A revised scheme for the reactivity of iron (oxyhydr)oxide minerals towards dissolved sulfide. *Geochim. Cosmochim. Acta* **68**, 3703–3715.

Raiswell R., Hardisty D. S., Lyons T. W., Canfield D. E., Owens J. D., Planavsky N. J., Poulton S. W. and Reinhard C. T. (2018) The iron paleoredox proxies: A guide to the pitfalls, problems and proper practice. *Am. J. Sci.* **318**, 491–526.

Reed D. C., Slomp C. P. and de Lange G. J. (2011) A quantitative reconstruction of organic matter and nutrient diagenesis in Mediterranean Sea sediments over the Holocene. *Geochim. Cosmochim. Acta* **75**, 5540–5558.

Reeder R. J., Nugent M., Tait C. D., Morris D. E., Heald S. M., Beck K. M., Hess W. P. and Lanzirotti A. (2001) Coprecipitation of Uranium(VI) with Calcite: XAFS, micro-XAS, and luminescence characterization. *Geochim. Cosmochim. Acta* **65**, 3491–3503.

Reitz A., Thomson J., de Lange G. J. and Hensen C. (2006) Source and development of large manganese enrichments above eastern Mediterranean sapropel S1. *Paleoceanography* **21**.

Rohling E., Marino G. and Grant K. (2015) Mediterranean climate and oceanography, and the periodic development of anoxic events (sapropels). *Earth-Sci. Rev.* **143**, 62–97.

Rolison J. M., Stirling C. H., Middag R. and Rijkenberg M. J. A. (2017) Uranium stable isotope fractionation in the Black Sea: Modern calibration of the $^{238}U/^{235}U$ paleoredox proxy. *Geochim. Cosmochim. Acta* **203**, 69–88.

Romaniello S. J., Herrmann A. D. and Anbar A. D. (2013) Uranium concentrations and $^{238}U/^{235}U$ isotope ratios in modern carbonates from the Bahamas: Assessing a novel paleoredox proxy. *Chem. Geol.* **362**, 305–316.

Slomp C., Van der Gaast S. and Van Raaphorst W. (1996) Phosphorus binding by poorly crystalline iron oxides in North Sea sediments. *Mar. Chem.* **52**, 55–73.

Stirling C. H., Andersen M. B., Potter E.-K. and Halliday A. N. (2007) Low-temperature isotopic fractionation of uranium. *Earth Planet. Sci. Lett.* **264**, 208–225.

Stirling C. H., Andersen M. B., Warthmann R. and Halliday A. N. (2015) Isotope fractionation of ^{238}U and ^{235}U during biologically-mediated uranium reduction. *Geochim. Cosmochim. Acta* **163**, 200–218.

Sturchio N., Antonio M., Soderholm L., Sutton S. and Brannon J. (1998) Tetravalent uranium in calcite. *Science* **281**, 971–973.

Sweere T., Hennekam R., Vance D. and Reichart G. J. (2021) Molybdenum isotope constraints on the temporal development of sulfidic conditions during Mediterranean sapropel intervals. *Geochem. Perspect. Lett.* **17**, 16–20.

Thomson J., Higgs N., Wilson T., Croudace I., De Lange G. and Van Santvoort P. (1995) Redistribution and geochemical behaviour of redox-sensitive elements around S1, the most recent eastern Mediterranean sapropel. *Geochim. Cosmochim. Acta* **59**, 3487–3501.

Thomson J., Jarvis I., Green D. R., Green D. A. and Clayton T. (1998) Mobility and immobility of redox-sensitive elements in deep-sea turbidites during shallow burial. *Geochim. Cosmochim. Acta* **62**, 643–656.

Thomson J., Mercone D., De Lange G. and Van Santvoort P. (1999) Review of recent advances in the interpretation of eastern Mediterranean sapropel S1 from geochemical evidence. *Mar. Geol.* **153**, 77–89.

Tissot F. L., Chen C., Go B. M., Naziemiec M., Healy G., Bekker A., Swart P. K. and Dauphas N. (2018) Controls of eustasy and diagenesis on the ^{238}U/^{235}U of carbonates and evolution of the seawater (^{234}U/^{238}U) during the last 1.4 Myr. *Geochim. Cosmochim. Acta* **242**, 233–265.

Tissot F. L. and Dauphas N. (2015) Uranium isotopic compositions of the crust and ocean: age corrections, U budget and global extent of modern anoxia. *Geochim. Cosmochim. Acta* **167**, 113–143.

Tribovillard N., Algeo T. J., Lyons T. and Riboulleau A. (2006) Trace metals as paleoredox and paleoproductivity proxies: an update. *Chem. Geol.* **232**, 12–32.

Twitchett R. J. and Wignall P. B. (1996) Trace fossils and the aftermath of the Permo-Triassic mass extinction: evidence from northern Italy. *Palaeogeogr., Palaeoclimatol., Palaeoecol.* **124**, 137–151.

Van Santvoort P., De Lange G., Thomson J., Cussen H., Wilson T., Krom M. and Ströhle K. (1996) Active post-depositional oxidation of the most recent sapropel (S1) in sediments of the eastern Mediterranean Sea. *Geochim. Cosmochim. Acta* **60**, 4007–4024.

Wang X., Johnson T. M. and Lundstrom C. C. (2015) Isotope fractionation during oxidation of tetravalent uranium by dissolved oxygen. *Geochim. Cosmochim. Acta* **150**, 160–170.

Weltje G. J., Bloemsma M., Tjallingii R., Heslop D., Röhl U. and Croudace I. W. (2015) *Prediction of geochemical composition from XRF core scanner data: a new multivariate approach including automatic selection of calibration samples and quantification of uncertainties, Micro-XRF Studies of Sediment Cores*. Springer, pp. 507–534.

Weyer S., Anbar A., Gerdes A., Gordon G., Algeo T. and Boyle E. (2008) Natural fractionation of ^{238}U/^{235}U. *Geochim. Cosmochim. Acta* **72**, 345–359.

Wignall P. B. and Newton R. (1998) Pyrite framboid diameter as a measure of oxygen deficiency in ancient mudrocks. *Am. J. Sci.* **298**, 537–552.

Zhang F., Lenton T. M., del Rey Á., Romaniello S. J., Chen X., Planavsky N. J., Clarkson M. O., Dahl T. W., Lau K. V. and Wang W. (2020) Uranium isotopes in marine carbonates as a global ocean paleoredox proxy: a critical review. *Geochim. Cosmochim. Acta* **287**, 27–49.

Zhao M.-Y., Zheng Y.-F. and Zhao Y.-Y. (2016) Seeking a geochemical identifier for authigenic carbonate. *Nat. Commun.* **7**, 10885.

Zheng Y., Anderson R. F., van Geen A. and Fleisher M. Q. (2002) Remobilization of authigenic uranium in marine sediments by bioturbation. *Geochim. Cosmochim. Acta* **66**, 1759–1772.

Associate editor: Stefan Weyer